



RESEARCH ARTICLE

10.1029/2021JD036012

This article is a companion to Gilbert et al. (2022), <https://doi.org/10.1029/2021JD034766>.

Key Points:

- The amount of surface melting on Larsen C is driven mostly by sunny conditions, followed by foehn events, cloud, and large-scale circulation
- Deep Amundsen Sea Low, positive Southern Annular Mode, and El Niño conditions enhance surface melting
- Drivers of surface melting overlap and interact

Supporting Information:

Supporting Information may be found in the online version of this article.

Correspondence to:

E. Gilbert,
ellgil82@bas.ac.uk

Citation:

Gilbert, E., Orr, A., Renfrew, I. A., King, J. C., & Lachlan-Cope, T. (2022). A 20-year study of melt processes over Larsen C ice shelf using a high-resolution regional atmospheric model: 2. Drivers of surface melting. *Journal of Geophysical Research: Atmospheres*, 127, e2021JD036012. <https://doi.org/10.1029/2021JD036012>

Received 11 OCT 2021

Accepted 4 APR 2022

Author Contributions:

Conceptualization: E. Gilbert, A. Orr, I. A. Renfrew, J. C. King

Formal analysis: E. Gilbert

Funding acquisition: A. Orr, I. A. Renfrew, J. C. King, T. Lachlan-Cope

Investigation: E. Gilbert, A. Orr, J. C. King

Methodology: E. Gilbert, A. Orr, I. A. Renfrew

Project Administration: E. Gilbert

Supervision: A. Orr, I. A. Renfrew, J. C. King, T. Lachlan-Cope

© 2022. The Authors.

This is an open access article under the terms of the [Creative Commons Attribution License](https://creativecommons.org/licenses/by/4.0/), which permits use, distribution and reproduction in any medium, provided the original work is properly cited.

A 20-Year Study of Melt Processes Over Larsen C Ice Shelf Using a High-Resolution Regional Atmospheric Model: 2. Drivers of Surface Melting

E. Gilbert^{1,2} , A. Orr¹ , I. A. Renfrew², J. C. King¹ , and T. Lachlan-Cope¹

¹British Antarctic Survey, Cambridge, UK, ²School of Environmental Sciences, University of East Anglia, Norwich, UK

Abstract Quantifying the relative importance of the atmospheric drivers of surface melting on the Larsen C ice shelf is critical in the context of recent and future climate change. Here, we present analysis of a new multidecadal, high-resolution model hindcast using the Met Office Unified Model, described in Part 1 of this study. We evaluate the contribution of various atmospheric conditions in order to identify and rank, for the first time, the most significant causes of melting over the recent past. We find the primary driver of surface melting on Larsen C is solar radiation. Foehn events are the second most important contributor to surface melting, especially in nonsummer seasons when less solar radiation is received at the surface of the ice shelf. Third, cloud influences surface melting via its impact on the surface energy balance (SEB); when the surface temperature is warm enough, cloud can initiate or prolong periods of melting. Lastly, large-scale circulation patterns such as the Southern Annular Mode (SAM), El Niño Southern Oscillation, and Amundsen Sea Low control surface melting on Larsen C by influencing the local meteorological conditions and SEB. These drivers of melting interact and overlap, e.g., the SAM influences the frequency of foehn, commonly associated with leeside cloud clearances and sunnier conditions. Ultimately, these drivers matter because sustained surface melting on Larsen C could destabilize the ice shelf via hydrofracturing, which would have consequences for the fate of the ice shelf and sea levels worldwide.

Plain Language Summary In order to predict the future of the largest remaining ice shelf on the Antarctic Peninsula—Larsen C—we must understand what is causing it to melt at the surface. We use results from a new model data set to explore which causes of melting are the most important. Our results show that the most dominant factor is solar radiation, especially in summer, while relatively warm, dry foehn winds are the second most important cause of melting. Foehn winds are an especially significant cause of melting in nonsummer seasons. The third driver of surface melting is cloud, because clouds can affect how much energy is received at the surface of the ice shelf. When it is warm enough, clouds can initiate or sustain melting. The final cause of melting is large-scale atmospheric circulation patterns, which can establish the conditions that promote melting, such as sunny, cloudy, or foehn periods. These melt drivers interact with one another and can compound or dampen the effects of other causes of melting. These melt drivers matter because surface melt could cause this ice shelf to collapse, and therefore indirectly contribute to sea level rise.

1. Introduction

Atmospheric drivers of surface melting were implicated in the collapse of the Larsen A and B ice shelves that previously neighbored Larsen C—the largest remaining ice shelf on the eastern side of the Antarctic Peninsula and which extends north of the Antarctic circle—by increasing firn densification, meltwater ponding, and ultimately hydrofracturing and disintegration (Bell et al., 2018; Scambos et al., 2000). In particular, the large-scale circumpolar westerly circulation is known to have an important role in the Antarctic Peninsula region by influencing local atmospheric conditions via its effect on foehn winds. Foehn winds cause leeside warming and associated melting over these ice shelves (Cape et al., 2015; Elvidge et al., 2015; King et al., 2017; Kuipers Munneke et al., 2018; Orr et al., 2008, 2021; van Lipzig et al., 2008), and a distinct west-east gradient in melting over Larsen C (Bevan et al., 2018; Elvidge et al., 2020; Gilbert et al., 2022). Large-scale circulation variability in the Southern Hemisphere is strongly influenced by the Southern Annular Mode (SAM). The SAM underwent a positive trend from the 1960s to the mid-1990s, particularly in austral summer (December, January, February—DJF), causing flow to be more dominantly westerly (Fogt & Marshall, 2020; Marshall, 2003; Marshall et al., 2006), although there has not been a significant trend since then. Stronger westerly flow associated with a more positive

Validation: E. Gilbert
Visualization: E. Gilbert
Writing – original draft: E. Gilbert
Writing – review & editing: E. Gilbert,
A. Orr, I. A. Renfrew, J. C. King

SAM strengthened the flow impinging on the Antarctic Peninsula, resulting in increased foehn-induced warming over the ice shelves (Cape et al., 2015; Datta et al., 2019; Orr et al., 2008).

The SAM is strongly correlated with the strength of the Amundsen Sea Low (ASL), which is a climatological low-pressure center in the Amundsen/Bellingshausen Seas to the west of the Antarctic Peninsula. The ASL influences near-surface wind, temperature, and sea ice concentration, and thus primarily temperatures on the western side of the Antarctic Peninsula (Hosking et al., 2013; King, 1994; Turner et al., 2013). The El Niño Southern Oscillation (ENSO) teleconnection also influences the ASL, primarily during austral winter (June, July, August—JJA) and spring (September, October, November—SON; Clem et al., 2016). The SAM and ENSO are shown to be anticorrelated throughout the instrumental record (Dätwyler et al., 2020; Fogt et al., 2011), and by influencing the strength of the ASL can affect the advection of warm maritime air across the Antarctic Peninsula and thus atmospheric conditions (including foehn events) over its eastern side.

The high mountains (~2,000 m) running along the spine of the Antarctic Peninsula present a significant barrier separating the relatively warm, maritime environment to the west from a much cooler continental climate on the eastern side (Orr et al., 2004). As well as acting as a barrier to prevailing westerly winds, cold air masses on the eastern side of the Antarctic Peninsula can also be blocked by the high orography, resulting in the formation of strong southerly or “barrier” winds flowing along the eastern side of the Peninsula (Parish, 1983; Schwerdtfeger, 1974), which can therefore affect temperatures over Larsen C.

Regional climate models (RCMs) are commonly used to assess the role of atmospheric drivers of melt on Larsen C due to the dearth of long-term observations (e.g., Datta et al., 2019; Elvidge et al., 2015, 2016, 2020; Gilbert et al., 2022; Kuipers Munneke et al., 2018; Laffin et al., 2021; Orr et al., 2008, 2021; Turton et al., 2018, 2020; Wiesenecker et al., 2019). However, many of these studies have focused on particular meteorological phenomena, especially the role of foehn winds (e.g., Datta et al., 2019; Laffin et al., 2021; Orr et al., 2008; Turton et al., 2018, 2020), and/or have examined melt over a relatively short timeframe (e.g., Elvidge et al., 2016, 2020; Gilbert et al., 2020; Kuipers Munneke et al., 2018). To date, no work has attempted to assess the relative importance of the first-order drivers of surface melting on Larsen C (i.e., SW radiation, foehn, cloud cover and phase, and large-scale circulation patterns like the SAM, ENSO, and ASL) on the surface energy balance (SEB) or melting over a multidecadal time period.

While van Wessem et al. (2015, 2016) produced near-surface climatologies of winds/temperatures and surface mass balance, respectively, over the Antarctic Peninsula using RACMO2.3 (Regional Atmospheric Climate Model) at a spatial resolution of 5.5 km, “significant biases” remained that the authors attribute to difficulties in resolving the steep topography that characterizes the region (van Wessem et al., 2016, p. 271). Resolving complex topography is vital for realistically simulating foehn winds, and may be more difficult using RACMO2.3 because its hydrostatic core prohibits the use of kilometer scale spatial resolution (Orr et al., 2008). It should be noted, however, that Wiesenecker et al. (2018) and Laffin et al. (2021) highlight RACMO2.3's satisfactory ability to resolve foehn events over Larsen C. Wiesenecker et al. (2019) diagnose foehn wind occurrence between 1979 and 2016 at Cabinet Inlet on Larsen C, situated close to the foot of the eastern slopes of the Antarctic Peninsula, from AWS and RACMO2.3 model data, but do not relate this to the SEB. King et al. (2015) comprehensively evaluate the ability of three RCMs to reproduce observed meteorology and SEB on Larsen C during summer 2010/11, but the period is short—just 1 month. Gilbert et al. (2020) evaluate melting on Larsen C over this same 1-month period but focus solely on the role of cloud on melt. Similarly, Elvidge et al. (2020) use the regional configuration of the UK Met Office Unified Model (MetUM) at 1.5-km resolution to assess the role of various SEB regimes in driving melt on Larsen C and include a thorough investigation of the role of solar radiation and foehn and the conditions that produce these, but this process-focused study is limited in its duration to 6 months. Datta et al. (2019) use the MAR (Modèle Atmosphérique Régionale) model at 7.5-km resolution to evaluate the effect of foehn events on the evolution of the snowpack during the period 1982–2017 and find three regimes in which surface melting occurs, related to foehn winds and cloud occurrence. However, the focus of their study is on the evolution of firn and the snowpack, rather than quantifying the atmospheric processes that influence the SEB regime and surface melting. Laffin et al. (2021) examine the impact of foehn winds on melting during 1979–2018 using machine learning and the RACMO2.3 model, and Turton et al. (2020) combine observations and model output from AMPS (Antarctic Mesoscale Prediction System) to explore seasonal patterns in foehn-driven surface melt. Lastly, Bozkurt et al. (2020) use the WRF (Weather Research and Forecasting) model at 15-km resolution to

produce a hindcast for the Antarctic Peninsula over the period 1991–2015, which again is insufficiently fine-scale to adequately resolve important features such as foehn winds.

Some attempts have been made to link specific atmospheric drivers to increased melting over the ice shelves on the eastern side of the Antarctic Peninsula using a variety of methods. For instance, Cape et al. (2015) use satellite and Automatic Weather Station (AWS) data to correlate monthly Antarctic Peninsula foehn occurrence with backscatter-derived surface melt and find the strongest relationships on the Larsen A and B ice shelves and in inlets in the northwest of Larsen C ice shelf. Kuipers Munneke et al. (2018) demonstrate that a foehn event drove enhanced surface melting across Larsen C during austral autumn (March, April, May—MAM) 2016. Elvidge et al. (2020) also find that foehn winds are the dominant meteorological driver of melt across Larsen C, with the primary cause of melting attributed to incoming shortwave (SW) radiation, a result also reported by Gilbert et al. (2020) for DJF 2011. Foehn events are commonly associated with leeside cloud clearance and thus enhanced SW radiation (e.g., Takane & Kusaka, 2011).

Gilbert et al. (2020) identify cloud phase as a crucial determinant of melting over Larsen C because optically thick clouds with larger ice or liquid water paths (IWP or LWP) decrease downward SW radiation and increase downward longwave (LW) radiation, and whether the cloud enhances or suppresses melt depends on the balance between these radiative effects (Hofer et al., 2019). Optically thick cloud is shown by Ghiz et al. (2021) to increase downward LW fluxes enough to initiate and prolong periods of melting in West Antarctica, while optically thin liquid-bearing cloud can also enhance melting by increasing the total downward radiative flux, a phenomenon also noted in Greenland by Bennartz et al. (2013). Although demonstrated for short periods (Gilbert et al., 2020), the importance of cloud-mediated melting on Larsen C has not been examined over multiple decades.

Given these knowledge gaps, the aim of this investigation is to robustly quantify the importance of the various drivers of Larsen C surface melting over a multidecadal period. This is critical for understanding Larsen C's stability in the context of past, present, and future change. For example, Trusel et al. (2015), Lai et al. (2020), and Gilbert and Kittel (2021) identify Larsen C as being vulnerable to hydrofracturing-mediated collapse as the climate warms. By bringing together the many atmospheric drivers or conditions that are demonstrably important in the region, such as foehn, cloud phase, and large-scale circulation variability, this study will comprehensively determine their impact on the SEB and surface melting over Larsen C.

We will do this by examining output from the high-resolution multidecadal MetUM hindcast of the Antarctic Peninsula described in Part 1 of this study (Gilbert et al., 2022), which included a validation of the model SEB against AWS measurements on Larsen C. Part 1 showed that the hindcast is capable of representing the foehn-induced east-west gradient in surface melting on Larsen C observed by satellites (Bevan et al., 2018), i.e., indicating that it is able to reasonably represent foehn-associated flow. It further shows that the model captures the observed frequency of foehn events over Larsen C, and adequately simulates near-surface meteorology. This hindcast is therefore a useful resource for studying the dominant conditions that influence surface melting on the Larsen C ice shelf.

2. Data and Methods

2.1. The SEB and Surface Melt

The influence of atmospheric processes on surface melting is quantified by examining their effect on the SEB, defined as the balance between upwelling and downwelling components of surface SW and LW radiation, SW_{\uparrow} , SW_{\downarrow} , LW_{\uparrow} , and LW_{\downarrow} , respectively, and the latent, sensible, and ground heat fluxes, H_S , H_L , and G_S , respectively, and which is formulated as

$$E_{tot} = LW_{\uparrow} + LW_{\downarrow} + SW_{\uparrow} + SW_{\downarrow} + H_S + H_L + G_S \quad (1)$$

where fluxes directed toward the snow surface are defined as positive. Surface melt energy, E_{melt} , is positive when the sum of fluxes, E_{tot} , is positive and surface temperature, T_S , is at or above the melting point, i.e.,

$$E_{melt} = \begin{cases} E_{tot} & T_S \geq 0^\circ\text{C} \\ 0 & T_S < 0^\circ\text{C} \end{cases} \quad (2)$$

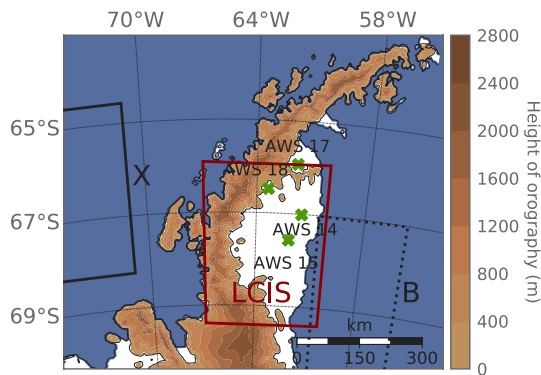


Figure 1. Map of the Antarctic Peninsula MetUM hindcast model domain, with the locations of the four Automatic Weather Stations (AWSs) used for validation indicated with green crosses. The map is centered on the Larsen C ice shelf and its tributary inlets, and also shows the remnant Larsen B ice shelf on which AWS 17 is located. The mean modeled height of orography is indicated with colored contours and is derived from the RAMP 200 m elevation model (Liu et al., 2015). The three regions used in the diagnosis of conditions influencing melt are also shown. Abbreviations used in the plot are as follows. “X”: region in which u_{z1} is calculated, used for diagnosing foehn conditions; “B”: region for diagnosing barrier wind conditions; “LCIS”: Larsen C box used to calculate means for high and low melt, high and low LWP, sunny, cloudy, and clear conditions.

2.2. The MetUM Model

As the MetUM hindcast is comprehensively described and evaluated in Gilbert et al. (2022), this section will only give brief details of the simulation. The hindcast uses a spatial resolution of 4 km over a domain that covers the central Antarctic Peninsula, centered on the Larsen C ice shelf (Figure 1). Boundary conditions are from ERA-Interim (Dee et al., 2011). It has output at three and six hourly temporal resolution for one/two-dimensional and three-dimensional variables, respectively. The variables archived include SEB terms (turbulent and radiative fluxes), near-surface meteorology (winds, humidity, temperatures, pressure, etc.), cloud fields (water paths, mass mixing ratios, cloud fractions, etc.) and surface melt terms as well as three-dimensional winds, potential temperature, air temperature, and specific humidity on model and pressure levels. A full description of the outputs can be found at Gilbert (2020a).

On average, Gilbert et al. (2022) found that the MetUM hindcast simulates conditions over Larsen C that are slightly warmer, windier, and moister compared to observations from AWSs, and that net surface radiation, R_{net} ($LW_{net} + SW_{net}$), and E_{melt} are under-estimated. The hindcast represents many components of the SEB well, e.g., model SW albedo is simulated to within 1% and 3% of observed values at inlet and ice shelf AWSs, respectively. Inlet stations are situated along the western edge of the ice shelf at the base of the Antarctic Peninsula, and ice shelf stations are situated over the homogeneous ice to the east of the Peninsula. Downwelling surface radiative fluxes are simulated within 10% of observed values at both inlet and ice shelf stations.

However, even small compensating errors in the downwelling fluxes, for instance related to errors in the simulated cloud field, have implications for interpreting the results. Positive T_s and consequently LW_{\uparrow} biases result in negative R_{net} and E_{melt} biases that are more pronounced at inlet stations, and during DJF. More detailed validation can be found in Part 1.

2.3. Diagnosing Dominant Conditions

The relative importance of various drivers of surface melting is assessed by examining periods when certain conditions prevail, which have been identified from the literature summarized in Section 1. These include: sunny, foehn, cloudy, clear, high/low LWP, barrier wind, ASL, positive/negative SAM, positive/negative ENSO, and high/low melt conditions. These are listed in Table 1 and defined in full below. Large-scale circulation patterns (i.e., SAM, ASL, and ENSO) are diagnosed using observed indices. All other conditions are determined from model output and diagnosed from “indicator variables,” which are the parameters that reveal whether or not certain conditions prevail. The regions used for averaging indicator variables are shown in Figure 1 and data sources and treatments are described in detail in Table 1.

Foehn conditions are diagnosed when foehn winds are detected in the model data for at least six 3-hr periods in a day at the locations of all of the three AWSs on the Larsen C ice shelf (AWS 14, 15, and 18; see Figure 1 for their location), which may indicate either foehn conditions occurring persistently at one AWS (i.e., for 18+ hours in a day) or foehn occurring at all three AWSs (i.e., for 6+ hours in a day), or a combination of these situations. Foehn events at each AWS location are detected using the isentrope-based method described in Gilbert et al. (2022), which diagnoses foehn conditions over Larsen C if the following occur: (a) the mean upstream zonal flow impinging on the Antarctic Peninsula between approximately 250–2,500 m altitude, u_{z1} , has a clear westerly component (i.e., $u_{z1} \geq 2 \text{ m s}^{-1}$) so that the oncoming flow can be forced over the Peninsula (Orr et al., 2008, 2021), (b) the upwind isentrope at altitude Z1 (~2,500 m) falls downstream of the Peninsula (over Larsen C) by an altitude of at least 500 m over a 6-hr period, and (c) warming of the atmospheric column is simulated over Larsen C, resulting in warming and drying at the ice shelf surface.

Table 1
Indicator Variables, Thresholds, and Regions Used in Diagnosing the Conditions Used for Compositing

Condition	Indicator variable	Threshold	Region
Low melt	Meltwater production	<25th percentile	Region “LCIS”
High melt	Meltwater production	>75th percentile	Region “LCIS”
Sunny	SW_{\downarrow}	>75th percentile	Region “LCIS”
Barrier wind	V wind	5.0 m s ⁻¹	Region “B”
Foehn	U wind, T_{air} , RH, potential temperature	≥6 3-hr periods of foehn at 3 AWSs (see main text for details)	u_{z1} calculated in region “X,” T_{air} and RH changes calculated in the grid box of interest
ASL	Hosking et al. (2013) index	Pressure anomaly below 25th percentile	Pressure center north of 70°S
SAM+	SAM index	+1σ (+1.36)	N/A
SAM−	SAM index	−1σ (−1.36)	N/A
ENSO+ (La Niña conditions)	Nino3.4 index	+0.5	N/A
ENSO− (El Niño conditions)	Nino3.4 index	−0.5	N/A

Note. Prevailing conditions are abbreviated as defined in the main text, where the acronyms “SAM,” “ENSO,” and “ASL” refer to the Southern Annular Mode, El Niño Southern Oscillation, and Amundsen Sea Low, respectively. The regions used are indicated in Figure 1. Note that high and low melt conditions are responses to forcing (such as foehn conditions or SW radiation) rather than causes of melting themselves and are used to guide the analysis in Section 3.

Sunny conditions are diagnosed when the mean incoming solar radiative flux (SW_{\downarrow}) over the Larsen C ice shelf (averaged over the region marked “LCIS” in Figure 1) exceeds the 75th percentile of 20-year mean SW_{\downarrow} for the day of the year considered. SW_{\downarrow} is therefore the “indicator variable” that enables the detection of these conditions. Cloudy and clear conditions are detected using cloud fraction, averaged over the “LCIS” region in Figure 1, according to the thresholds of Kay et al. (2008). “Cloudy” conditions are diagnosed when the mean cloud fraction exceeds 0.75, while “clear” conditions occur when cloud fraction is below 0.31. High and low LWP conditions occur when the mean LWP over the “LCIS” region falls above and below the 75th and 25th percentiles for that day of the year, respectively, in a manner similar to the diagnosis of sunny conditions. High and low IWP conditions are not examined because liquid cloud was shown to exert a more important control on the SEB and surface melting over Larsen C in Gilbert et al. (2020).

Barrier wind conditions are diagnosed when mean 10 m meridional wind speeds in the Weddell Sea region (marked “B” in Figure 1) exceed 5 m s⁻¹, indicative of strong near-surface southerly flow. Modeled 20-year mean meridional wind speeds in this region are 1.13 m s⁻¹, so this threshold represents a significant increase. High and low melt periods are determined using the 75th and 25th percentiles of meltwater production, respectively, averaged over the “LCIS” region.

The daily mean SAM index is that of the US National Oceanic and Atmospheric Administration (NOAA)'s National Weather Service Climate Prediction Centre and is calculated from National Center for Environmental Prediction/National Center for Atmospheric Research reanalysis at 2.5° × 2.5° resolution (CCP, 2005). Positive and negative SAM periods are abbreviated as “SAM+” and “SAM−,” respectively. The Nino3.4 data set (Reynolds et al., 2007), which is used by the World Meteorological Organization and NOAA to diagnose El Niño and La Niña events, is used to diagnose the phase of ENSO at daily frequency. El Niño and La Niña periods are abbreviated to “ENSO−” and “ENSO+,” respectively. Positive and negative phases of these circulation modes are detected when the index is above/below plus/minus one standard deviation of the time series 1998–2017. Positive and negative ENSO periods are diagnosed when 3-month running mean anomalies are above or below 0.5 or −0.5 °C, respectively, according to the method of NOAA (see <https://www.weather.gov/fwd/indices>, accessed 30 June 2020).

The influence of the ASL is examined using the observed index of Hosking et al. (2013), which measures the depth and longitude of the ASL. Deep ASL conditions (hereafter referred to simply as “ASL conditions”) are diagnosed when the relative central pressure is less than the 25th percentile and its latitude is north of 70°S, where it will have a more notable impact on conditions over Larsen C. (Here the relative central pressure is defined by subtracting the actual central pressure from an area-averaged pressure over the ASL sector, defined as 170°–298°E, 80°–60°S, see Hosking et al., 2013).

2.4. Analysis Methods

The study employs two primary analysis methods. First, Pearson correlation coefficients (r values) between pertinent variables (such as E_{melt} and SW_{\downarrow}) are examined to quantify the strength of the relationships between modeled variables. The statistical significance of the relationship is also calculated as a two-sided p value. Second, a composite approach is used, in a similar manner to Deb et al. (2018). During periods when particular conditions are diagnosed as described above, mean meteorological variables (3-hourly mean 10 m winds, 1.5 m air temperature, and MSLP) and SEB parameters (SW , LW , H_S , H_L , E_{tot} , and E_{melt}) are averaged to produce a composite that represents the meteorological state during these conditions. The relative proportion of total melt produced during conditions characteristic of each melt driver, as well as the proportion of time in which those conditions occur, were also calculated in order to quantify the importance of each driver of surface melt on Larsen C. All analysis was performed seasonally and is based on model output for the 1998–2017 period.

3. Results and Discussion

The drivers of surface melting are first considered by examining the “high melt” composites. After this, we assess the role of the most important controls on surface melt.

3.1. “High Melt” Composites

Figure 2 shows composited mean seasonal conditions during high melt conditions (melt amount >75th percentile, Table 2); panels a–c show daily near-surface meteorological conditions, while daily E_{melt} anomalies relative to the climatology for 1998–2017 are shown in panels d–f. Figure 2 shows that for all seasons, instances of high melting over Larsen C occur during periods of north-westerly flow, which produces cross-peninsula winds and therefore is conducive to establishing foehn conditions, and/or the advection of relatively warm and moist maritime air across the Antarctic Peninsula.

Consistent with Kuipers Munneke et al. (2018) and Elvidge et al. (2020), these conditions are associated with significant increases in H_S (not shown), and consequently in E_{tot} and E_{melt} over Larsen C, driving surface melting particularly during DJF when surface temperature is higher. During DJF high melt conditions are associated with high SW_{\downarrow} fluxes, causing temperatures to be at the melt point more frequently. Compared to the other seasons, DJF is also associated with comparatively weaker cross-peninsula flow and comparatively small T_{max} anomalies (Figure 2b). Around 63% of DJF meltwater production over Larsen C occurs in high melt periods (Table 2), which take place over the entire ice shelf (Figure 2e). This differs from SON, MAM, and JJA, when melting occurs almost exclusively during intense melt events (Kuipers Munneke et al., 2018) associated with cross-peninsula flow and is confined to the western regions of the ice shelf (Figures 2d and 2f, JJA not shown), with 93%, 98%, and 97% of seasonal meltwater production occurring in just 9%, 7%, and <1% of the time, respectively (Table 2).

The following subsections examine in turn the role of each of the various conditions described in Section 2.3 on surface melt over Larsen C.

3.2. Drivers of Modeled Surface Meltwater Production

3.2.1. Solar Radiation

Table 3 shows Pearson correlation coefficients between daily E_{melt} and other SEB components over the Larsen C ice shelf for the entire hindcast period. The largest annual correlation between E_{melt} and the fluxes in Table 3 is with net SW radiation, SW_{net} ($r_{SW_{net}, melt} = 0.56$). This relationship is also seen in DJF ($r_{SW_{net}, melt} = 0.45$), which supports the findings of Gilbert et al. (2020) that SW radiation is a dominant driver of summertime surface melting. Ninety percent of hindcast-simulated surface melting occurs in DJF (not shown) when SW_{\downarrow} is highest, which suggests that meltwater production is driven predominantly by SW_{\downarrow} . This result is consistent with Elvidge et al. (2020) and Gilbert (2020b), who also find that SW radiation is the dominant cause of surface melting during summer. Correlations are insignificant in JJA (Table 3) when there is very little SW_{\downarrow} and <0.1% of meltwater production occurs. For this reason, JJA is not included in Figure 2 or subsequent composite figures.

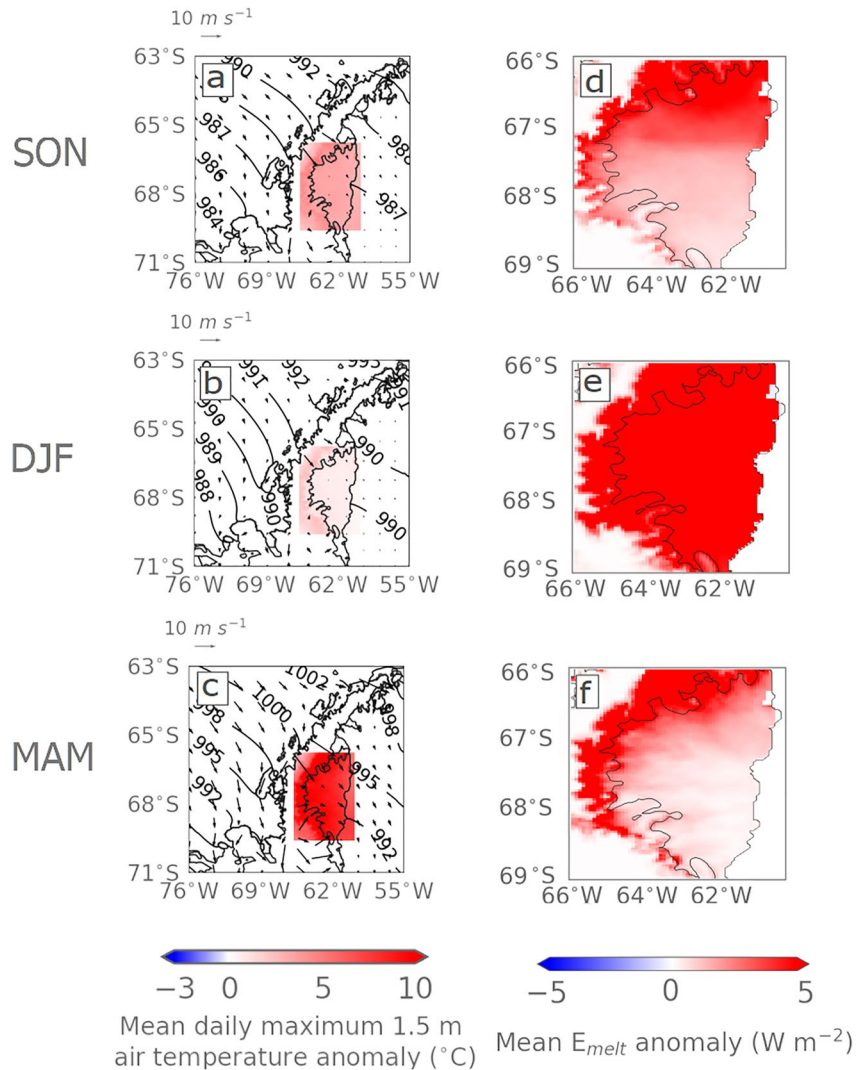


Figure 2. Compositing daily mean conditions during "high melt" conditions (melt amount >75th percentile) for spring (SON), summer (DJF), and autumn (MAM), for the hindcast period. JJA is not shown because the amount of melting occurring during winter is negligible. Panels (a)–(c) show mean synoptic meteorological conditions, where colored shading shows the daily maximum 1.5 m air temperature anomaly (T_{max} ; units °C), and contours and vectors give mean sea level pressure (hPa) and 10 m wind speed and direction, respectively. Panels (d)–(f) show anomalies in surface melt (E_{melt} ; units $W m^{-2}$). Anomalies are computed relative to the 1998–2017 model climatology. Synoptic meteorology plots show the wider Antarctic Peninsula region, while the E_{melt} plots focus on the Larsen C ice shelf.

Table 2 shows that "sunny" conditions ($SW_{\downarrow} > 75$ th percentile) occur 25% of the time in DJF, yet account for 42% of total DJF meltwater production (and around 38% of the annual total, not shown in Table 2). The proportion of meltwater production associated with "sunny" conditions increases to 47% and 75% in MAM and SON, respectively (Table 2), indicating that periods of above-average insolation are important for driving surface melt during these seasons, particularly during SON. Once the frequency of occurrence is accounted for, "sunny" conditions account for the highest percentage of meltwater production of any driver in DJF and SON. This is also apparent from Figure 3, which shows that the largest DJF E_{melt} anomalies are associated with "sunny" conditions. "Sunny" conditions are associated with extensive positive E_{melt} anomalies across the ice shelf, especially during DJF (Figure 3m) but also during SON (Figure 3j), partly because extensive T_{max} anomalies occur during such periods, especially in DJF (Figure 3d).

The co-occurrence of "high melt" and "sunny" conditions can also be used to demonstrate the importance of SW radiation in driving more intense melt events. During SON, DJF and MAM, "high melt" and "sunny" conditions

Table 2

Percentage of Total Modeled Meltwater Production (%) Associated With the Conditions Evaluated During Each Season for the Hindcast Period, and the Frequency at Which They Occur (%)

	DJF		MAM		JJA		SON	
	Melt amount	Frequency						
Low melt	0.8	24.5	0.0	7.1	0.1	0.6	0.1	9.1
High melt	63.0	24.5	97.6	7.2	96.7	0.7	92.5	9.1
Sunny	41.7	25.0	47.1	25.0	0.3	25.0	75.2	25.0
Foehn	22.4	18.7	54.8	16.7	97.3	20.9	47.6	23.7
Cloudy	50.2	61.6	69.1	54.6	95.5	56.9	56.6	61.7
Clear	9.8	7.8	2.4	9.2	0.0	10.8	4.2	6.9
Low LWP	32.0	25.0	4.2	25.0	0.0	25.0	8.4	25.0
High LWP	15.2	25.0	44.4	25.0	90.7	25.0	35.7	25.0
SAM+	25.0	21.9	38.9	17.3	21.9	22.2	24.5	16.9
SAM−	8.5	9.3	0.5	10.7	0.1	15.6	10.9	16.4
ENSO+	38.1	40.0	17.1	35.5	1.5	15.3	34.7	27.3
ENSO−	34.6	33.5	65.6	23.2	3.8	15.2	29.5	28.1
ASL	6.4	3.3	19.9	11.7	0.2	11.6	19.4	36.6
Barrier	3.8	10.8	0.0	15.9	0.0	19.2	1.4	18.3

co-occur 73%, 50%, and 46% of the time, respectively (not shown). The high co-occurrence during SON suggests that SW radiation is especially important for driving the most intense melt events, whereas high melt periods in DJF when SW_{\downarrow} is more similar to climatological conditions can still account for a comparatively large amount of melting. Because 96% of total annual melt occurs during these two seasons, these results suggest that SW radiation is the most important driver of surface melting on Larsen C overall.

3.2.2. Foehn

The frequency of foehn events at inlet and ice shelf stations is diagnosed using the isentropo-based method described in Section 2.3 and composites of near-surface meteorology and surface fluxes when foehn winds are detected are shown in the second column of Figure 3. Foehn conditions are associated with strong north-westerly flow and positive T_{max} anomalies in all seasons (Figures 3b, 3e, and 3h), which has different effects on E_{melt} in different seasons (Figures 3k, 3n, and 3q). During JJA (not shown), temperatures are largely too low for melting to occur. In contrast, in DJF foehn events are associated with positive E_{melt} anomalies that are distributed fairly evenly across Larsen C (Figure 3n), with slightly higher anomalies in inlets below the peaks in orography, i.e., there is a zonal gradient in melt. E_{melt} anomalies in SON (Figure 3k) are similarly extensive, but of lower magnitude, whereas much more intense, confined melting is simulated in the immediate lee of steep topography in MAM (Figure 3q).

Using the isentropo-based method, foehn conditions are diagnosed 92%, 49%, 40%, and 24% of the time that “high melt” conditions shown in Figure 2 also occur in JJA, MAM, SON, and DJF, respectively (not shown). Foehn are less important for driving intense melt events in DJF because foehn occur less frequently (19% of the time, Table 2) and have less impact (accounting for 22% of melt, Table 2) because SW radiation is the primary driver of melting in summer and temperatures are already closer to the melting point. This is evident in Figure 3 from the lower T_{max} anomalies associated with foehn conditions in DJF (panels b, e, and h). As shown in Section 3.2.1, SW radiation is the most important driver of intense melt events in SON (Figure 3j), although the foehn conditions are still associated with 48% of SON melt

Table 3

Pearson Correlation Coefficients (r) Between E_{melt} and SW_{\downarrow} , SW_{net} , LW_{\downarrow} , LW_{net} , H_S , and H_L Over the Larsen C Ice Shelf During Each Season, and Annually, for the Hindcast Period

	DJF	MAM	JJA	SON	ANN
SW_{\downarrow}	0.42	—	—	0.29	0.52
SW_{net}	0.45	—	—	0.33	0.56
LW_{\downarrow}	—	0.15	—	0.22	0.33
LW_{net}	−0.19	—	—	—	−0.12
H_S	0.38	0.28	0.11	—	—
H_L	0.15	0.08	—	−0.14	−0.19

Note. Only values that are significant at the 99% level are shown.

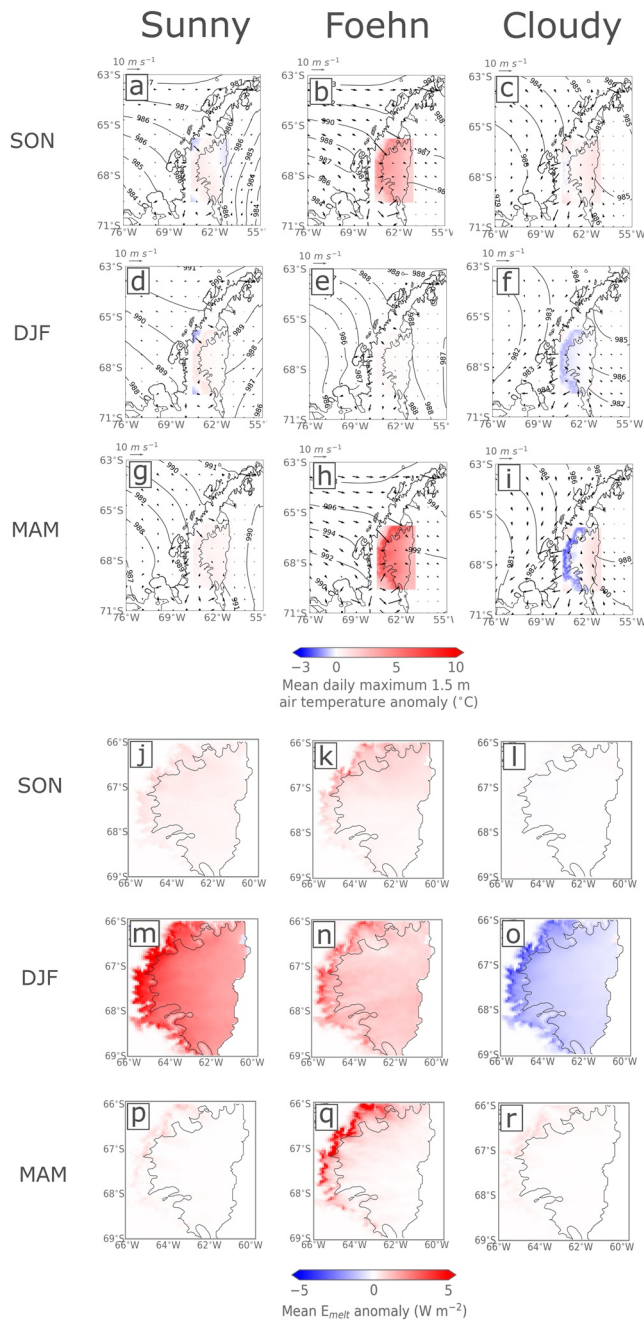


Figure 3. As in Figure 2 but showing composited mean synoptic near-surface meteorology (panels a–i) and E_{melt} fluxes (panels j–r) in “sunny” (first column), “foehn” (second column), and “cloudy” (third column) conditions during SON (first and fourth rows), DJF (second and fifth rows), and MAM (third and sixth rows) for the hindcast period. JJA is not shown because $<0.1\%$ of melting occurs during winter. Contours, vectors, colors, and shading are as in Figure 2.

despite occurring only 24% of the time (Table 2). During MAM, foehn is far more important than SW, with “foehn” conditions associated with 55% of MAM melting, despite occurring just 17% of the time (Table 2). This is also apparent from Figures 3 (panels p and q) and 4.

The above results show that foehn events are an important driver of surface melting over the Larsen C ice shelf year-round but are especially important in nonsummer seasons. As discussed earlier, foehn events are associated with positive H_S fluxes because they bring warm air to the surface. Accordingly, positive correlations are simulated between E_{melt} and H_S in DJF, JJA, and MAM (Table 3), although these are larger during DJF and MAM. This result is consistent with Elvidge et al. (2020), who find that regimes dominated by large positive H_S fluxes account for a large amount of melting in nonsummer seasons, and that 76% of melting during foehn conditions occurred when H_S fluxes were large. The combined effect of foehn and warmer air temperatures may explain why the correlation between E_{melt} and H_S is higher in the warmer seasons of DJF and MAM (Table 3). The negative correlation between E_{melt} and H_L during SON and ANN ($r_{HL,melt} = -0.14$ and -0.19 , respectively, Table 3) suggests that melting in these seasons primarily occurs when air is anomalously warm and dry, driving upward (i.e., negative) H_L fluxes, consistent with foehn conditions. The weak correlation coefficients given in Table 3 between E_{melt} and the turbulent heat fluxes, which are themselves only a proxy for foehn events, cannot conclusively demonstrate the importance of foehn in driving surface melting. However, they add weight to the evidence presented above.

Figure 4 shows mean E_{melt} anomalies in seasons SON, DJF, and MAM for “sunny foehn,” “nonsunny foehn,” and “sunny nonfoehn” conditions, which allows us to further elucidate the relative importance of SW and foehn on melting over Larsen C. In all seasons, “sunny foehn” conditions account for more positive E_{melt} anomalies than either “sunny” or “foehn” conditions alone (e.g., compare Figures 3j, 3m, 3p, and 3k, 3n, 3q with Figures 4a–4c). In DJF, foehn conditions slightly enhance melting in inlets (Figure 3n), but SW radiation is evidently much more important for driving melt across the ice shelf because when SW_{\downarrow} is low, foehn conditions are associated with negative E_{melt} anomalies across much of Larsen C (Figure 4e). However, in MAM, the opposite is true, suggesting that foehn conditions are a more important driver of melt in this season than SW radiation: even when $SW_{\downarrow} > 75$ th percentile, if foehn conditions are not also simulated, E_{melt} anomalies are negative (Figure 4i). In SON, both foehn and sunny conditions must be simulated to generate positive E_{melt} anomalies. E_{melt} anomalies are negative during “nonsunny foehn” and “sunny nonfoehn” conditions (Figures 4d and 4g), but positive in “sunny foehn” (Figure 4a), which is consistent with the small positive E_{melt} anomalies associated with both “foehn” and “sunny” shown in Figures 3j and 3k.

3.2.3. Cloud

To examine the role of cloud on surface melting, composites of “cloudy” conditions are shown in the third column of Figure 3. During DJF, cloudy conditions are associated with an easterly flow of maritime air from the Weddell Sea and negative T_{max} anomalies on Larsen C (Figure 3f). This part of the Weddell Sea is typically ice-free during summer, so relatively warm, moist maritime air is advected over the cold ice shelf, resulting in cooling of the air and condensation. Further examination of the hindcast output shows that enhanced LW_{\downarrow} produces positive E_{tot} anomalies and a mean absolute value of 9.3 W m^{-2} over ice shelf areas away from the inlets, but because temperatures typically do not reach

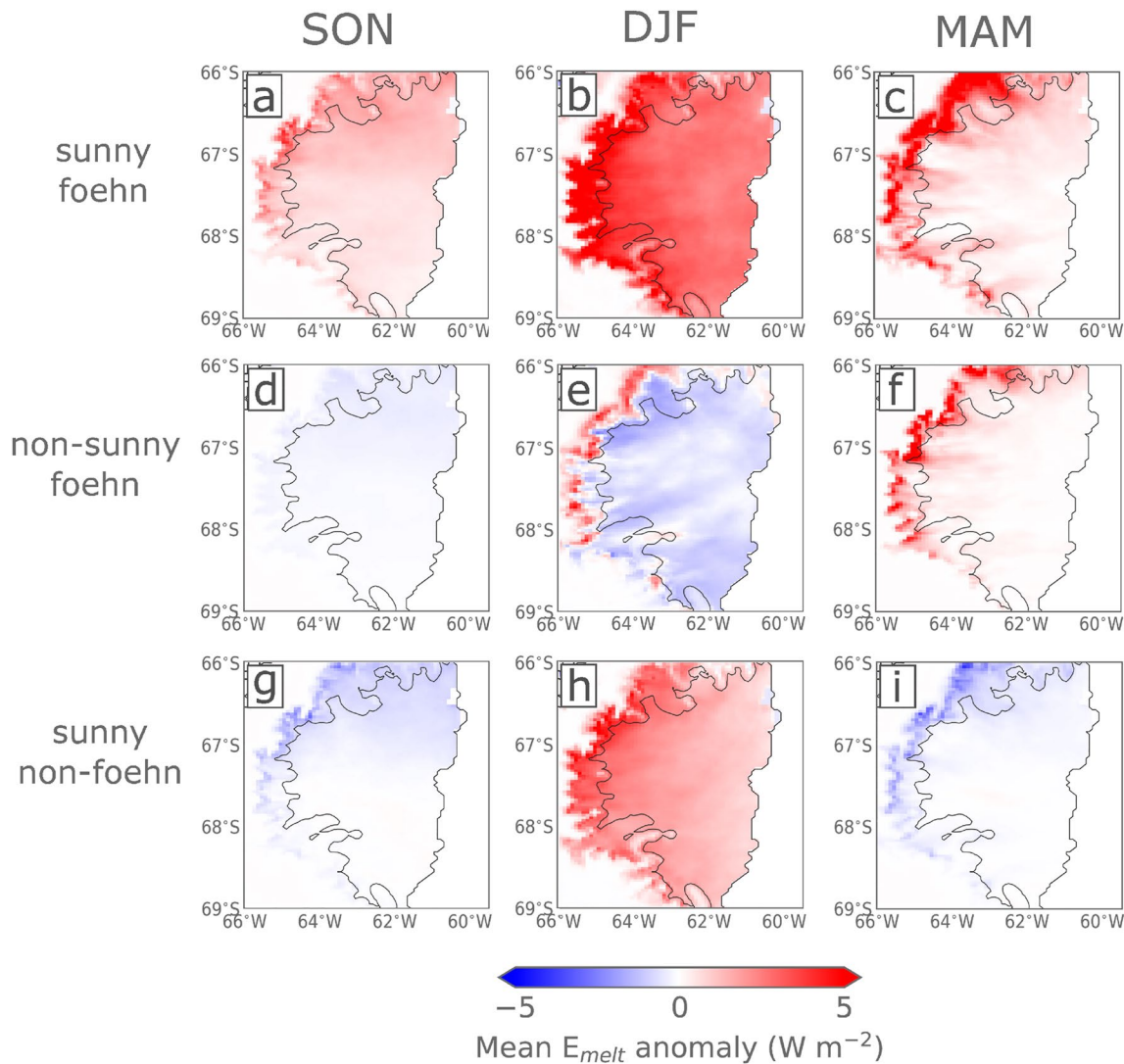


Figure 4. As in Figure 2, but showing seasonal E_{melt} anomalies only for SON (first column), DJF (second column), and MAM (third column) during three separate conditions for the hindcast period: “sunny foehn” when $SW_l > 75$ th percentile and foehn conditions are simulated (panels a–c); “nonsunny foehn” when foehn conditions are simulated but $SW_l < 25$ th percentile (panels d–f); and “sunny nonfoehn” when $SW_l > 75$ th percentile is simulated but foehn conditions are not (panels g–i).

the melting point during cloudy periods (mean T_{max} during “cloudy” conditions is around -1.1 °C), and because SW_l is reduced, melt anomalies are negative (Figure 3o). Therefore, despite occurring 62% of the time in DJF, “cloudy” conditions are associated with just 50% of melt (Table 2). SON composites (Figures 3c and 3l) mirror the DJF composites, with cloudy conditions suppressing melt relative to the climatology. Cloudy conditions occur 62% of the time in SON but are associated with just 57% of melt (Table 2).

During JJA, cloudy conditions, generated by cyclonic flow to the east and southerly winds over Larsen C, are associated with positive T_{max} anomalies (not shown). Table 2 shows that E_{melt} anomalies in JJA are almost zero because melt occurs so infrequently in JJA, but 95% of the melting that does occur is associated with cloudy conditions (91% for high LWP, Table 2). Cloudy composites during MAM (Figures 3i and 3r) are comparable to those during JJA, with cloud enhancing E_{melt} : 69% of MAM melting occurs in cloudy periods, which occur 55% of the time (Table 2).

Cloudy and clear conditions are typified by high and low liquid water path ($LWP > 75$ th percentile and < 25 th percentile), respectively, and synoptic conditions and SEB anomalies during “cloudy” conditions are virtually

indistinguishable from those during the “high LWP” regime (not shown), suggesting the prevalence of liquid-bearing cloud in the hindcast and its importance in determining melt. To avoid repetition, we do not include figures showing high LWP conditions because they are so similar.

The seasonal pattern outlined above is consistent with the correlation coefficients shown in Table 2, which show that E_{melt} is positively correlated with LW_{\downarrow} in MAM, SON, and annually ($r_{LW_{\downarrow},melt} = 0.15, 0.22, \text{ and } 0.33$, respectively). This supports the notion that LW_{\downarrow} is an important cloud-mediated control on surface melting, as demonstrated by, e.g., Zhang et al. (1996) and Gilbert et al. (2020). Cloudy, high LWP conditions may also induce a “thermal blanketing” effect, whereby SW_{\downarrow} is attenuated and LW_{\downarrow} enhanced so that R_{net} is close to zero or just positive. In these conditions, if H_S and surface temperatures are above zero, melting can result (Ghiz et al., 2021).

Because mean daily T_{max} during cloudy, high LWP conditions is only slightly below the melting point (as noted above) and the large LW_{\downarrow} fluxes associated with cloud produce positive E_{tot} fluxes, this implies that cloud could become an important driver of surface melt in a warming climate. Surface air temperatures on the eastern Antarctic Peninsula are projected to warm by $\sim 0.5\text{--}3\text{ }^{\circ}\text{C}$ by 2,100 and could warm considerably more even under $1.5\text{ }^{\circ}\text{C}$ global mean temperature rise (Siegert et al., 2019; van Oldenborgh et al., 2013), which would mean the melting point could be reached more frequently in DJF during cloudy periods. This could allow extensive low cloud-mediated melt events to occur such as were observed in Greenland in 2012 (Bennartz et al., 2013) and which have been documented in West Antarctica (Ghiz et al., 2021). As shown in Gilbert et al. (2020), cloud initiates summertime melt by raising surface temperatures and producing an energy surplus (positive E_{tot}), which then persists as cloud glaciation occurs and SW fluxes increase. This can induce a positive feedback if melt occurs in sufficient volume to reduce the surface albedo, because the darker melting surface can then absorb more SW radiation and sustain further melting. Because low-level (liquid) cloud is typically extensive on Larsen C, this melting could occur across the entire ice shelf.

3.2.4. Foehn-Induced Cloud Clearance on Larsen C

The various combinations of “sunny,” “clear,” “LWP25,” and “foehn” conditions can also be used to examine the importance of cloud clearance on Larsen C, whereby warm, dry foehn air reduces cloud cover and enhances melting by increasing SW_{\downarrow} (Hoinka, 1985). While this mechanism has been proposed to explain enhanced melting over the ice shelf, e.g., by Kuipers Munneke et al. (2012), Grosvenor et al. (2014), Cape et al. (2015), King et al. (2017), and Elvidge et al. (2020), its significance has not yet been established across larger spatial and temporal scales on Larsen C.

Foehn clearance can be defined as clear, sunny foehn periods with low LWP, or the coincidence of foehn conditions with any of these criteria. Because model cloud fraction is parameterized according to subgrid scale variability in moisture, it can be less reliable than prognostic diagnostics like LWP or solar radiation, so the definition is not necessarily as straightforward as the coincidence of clear and foehn periods. Of the times when foehn conditions are detected, “sunny” conditions also occur 27%, 29%, and 31% of the time in MAM, SON, and DJF, respectively (Table S1). Because cloudy conditions are so common on Larsen C (occurring 55–62% of the time, as shown in Table 2), “cloudy foehn” conditions also occur frequently, accounting for 35–59% of foehn periods depending on the season. “Clear foehn” occur on average approximately five times less frequently (9–13% of foehn periods, Table S1). “Low LWP foehn,” which may include foehn periods where optically thin liquid clouds or high-level ice clouds are present, account for 25–31% of foehn periods and 12–20% of foehn periods are “high LWP foehn” (Table S1).

Table 4 shows how frequently high melt periods coincide with these conditions. Figure 5 summarizes the dominant combinations of conditions that occur during “high melt” conditions in different seasons, and can be thought of as illustrating some of the primary “modes” of melting over Larsen C. Sunny conditions co-occur with 46–73% of high melt periods (excluding JJA when SW radiation is negligible; Figures 5a and 5g), while foehn and cloudy conditions co-occur with 24–92% and 44–85% of high melt periods, respectively (Table 4, Figures 5c and 5f). Clear and high melt conditions co-occur relatively infrequently, coinciding for <10% of the time high melt periods are detected in all seasons, consistent with clear conditions occurring infrequently (7–11% of the time in Table 2). Similarly, in nonsummer seasons low LWP periods coincide quite rarely with high melt periods (8% in MAM and 9% in SON, Table 4). In comparison, cloudy/high LWP conditions coincide with a much larger percentage of high melt periods than clear/low LWP conditions (Table 4 and Figure 5e). In DJF, however, while cloudy conditions coincide with a large proportion (44%) of high melt periods, high LWP conditions do not. Instead, low LWP

Table 4
Co-occurrence of “Sunny,” “Cloudy,” “Clear,” “High LWP,” “Low LWP,” and “Foehn” Conditions With “High Melt” Conditions During Each Season

	DJF (%)	MAM (%)	JJA (%)	SON (%)
Sunny	49.9	45.5	0.0	73.3
Foehn	23.7	48.5	92.3	40.6
Cloudy	44.2	50.8	84.6	54.5
Clear	9.7	5.3	0.0	6.1
High LWP	9.9	34.1	69.2	40.0
Low LWP	35.2	8.3	0.0	8.5
Sunny foehn (sunny + foehn)	12.9	18.2	0.0	27.9
Clear foehn (clear + foehn)	3.4	3.0	0.0	4.8
Cloudy foehn (cloudy + foehn)	10.6	20.5	76.9	20.6
Low LWP foehn (LWP25 + foehn)	9.3	6.1	0.0	3.6
High LWP foehn (LWP75 + foehn)	2.0	10.6	61.5	12.1

Note. The values shown represent the percentage of time during which the conditions overlap with high melt conditions, i.e., of the times that high melt conditions are occurring, what percentage of the time the conditions in question also occur.

and high melt conditions more commonly co-occur (35%). The importance of cloudy *and* low LWP conditions suggests that optically thin, low-level clouds could be important for driving surface melting over Larsen C during summer, as seen in Greenland and West Antarctica (Bennartz et al., 2013; Ghiz et al., 2021; Figure 5b), or that cloud clearance at lower levels could drive melting while high-level ice cloud is present (therefore resulting in a large cloud fraction, Figure 5c). The latter would constitute cloud clearance but further investigation is required.

In DJF, when the majority of melting occurs, E_{melt} anomalies averaged across the whole ice shelf are positive during “sunny foehn,” “low LWP foehn,” and “clear foehn” (1.00, 0.70, and 0.62 W m⁻², respectively, Table S1), and near-zero or negative during “cloudy foehn” and “high LWP foehn” (0.02 and -0.32 W m⁻², respectively, Table S1). In other seasons, the largest positive E_{melt} anomalies are associated with cloudy foehn and high LWP foehn (1.02 and 2.03 W m⁻², respectively, in MAM and 0.31 and 0.54 W m⁻², respectively, in SON, Table S1 in Supporting Information, Figure 5f).

Periods when all three criteria (“clear foehn,” “low LWP foehn,” and “sunny foehn”) occur together are uncommon, happening during <1% of the hindcast. However, these periods coincide with 1–4% of high melt periods (not shown), implying that foehn-induced cloud clearance may drive above-average summertime melt when it occurs, but that such conditions occur fairly infrequently. Further examination of the importance of foehn clearance is needed to comprehensively evaluate its role in driving melt.

3.2.5. The Influence of Large-Scale Circulation

While the most important first-order processes driving surface melting are SW radiation, foehn and cloud, large-scale circulation variations—associated with patterns like the SAM, ENSO, and ASL—exert controls on these processes. For example, the high melt years identified in Part 1 were also SAM+ years, supporting the idea that this atmospheric circulation pattern enhances melting. Table 2 suggests that SAM+ and ENSO- enhance surface melting in DJF and MAM, because the percentage of melt that is associated with them is higher than the percentage of time they occur. Meanwhile SAM-, ENSO+, and ASL conditions suppress melting in all seasons except for ENSO+ in SON (Table 2). This anticorrelation of ENSO/SAM modes (i.e., the co-occurrence of ENSO- and SAM+ conditions and vice versa) is consistent with the findings of, e.g., Fogt et al. (2011) and Dätwyler et al. (2020) noted in Section 1. As discussed in Section 1, ASL conditions strengthen the flow impinging on the Antarctic Peninsula and so can increase the advection of air over the peninsula mountains (Hosking et al., 2013), therefore enhancing melt over Larsen C.

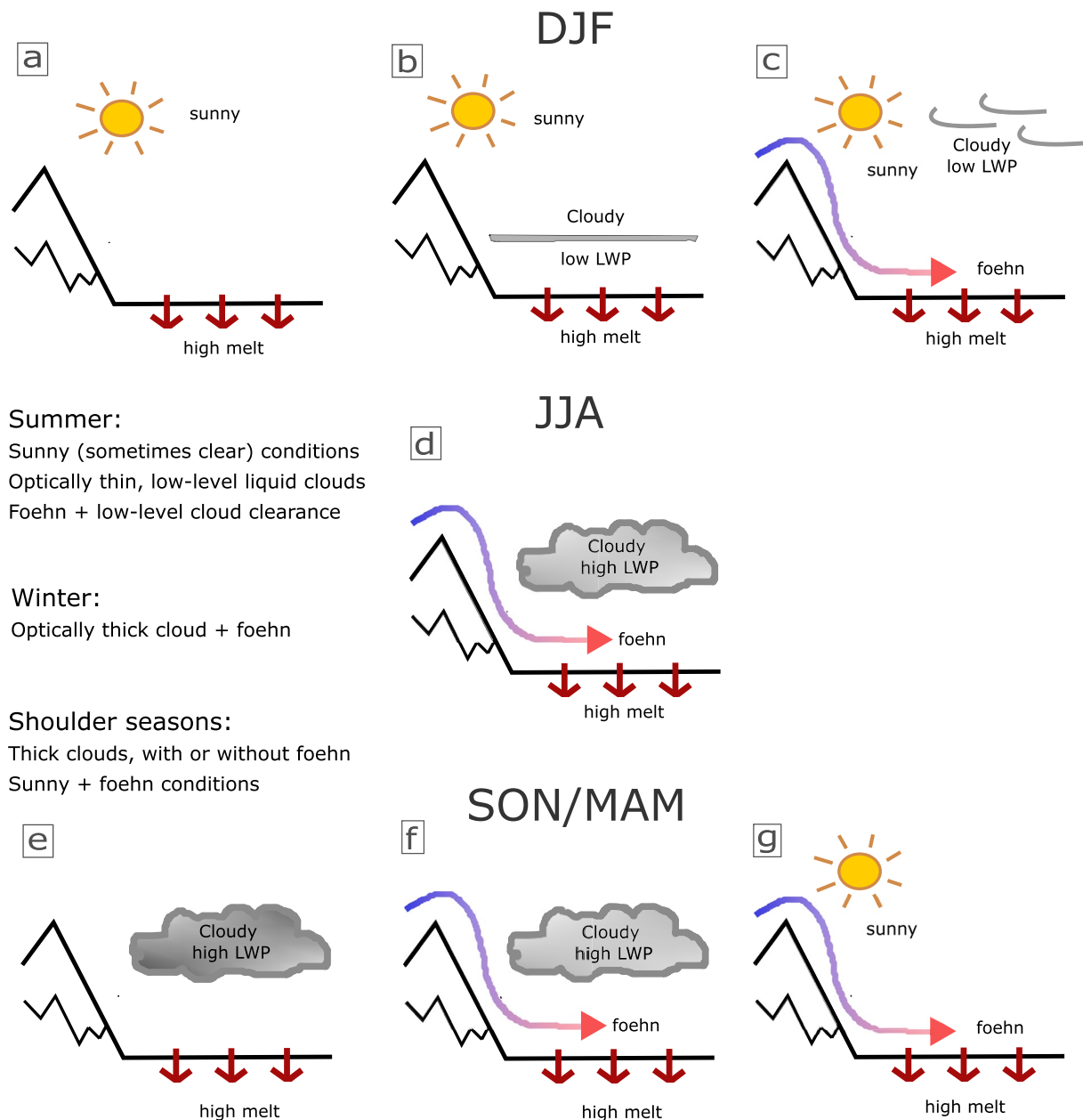


Figure 5. Schematic diagram illustrating the co-occurrence of various conditions and dominant modes of melting during each season. Note that melting in JJA occurs extremely infrequently and is associated with very small E_{melt} fluxes when it does occur.

Figure 6 shows composited mean meteorological conditions and E_{melt} anomalies during SAM+, SAM-, ENSO+, ENSO-, barrier wind, and ASL conditions. Anomalies are shown for DJF only, when their absolute influence on E_{melt} is strongest, although they have a larger relative effect on circulation and melting in other seasons. Comparing panels 6d and 6j further confirms that SAM+ and SAM- conditions produce positive and negative E_{melt} anomalies, respectively, especially in the immediate lee of steep terrain. Figures 6c and 6e also show that the circulation patterns in DJF associated with SAM+ and ENSO- are very similar, with weak cyclonic flow west of the Antarctic Peninsula generating weak cross-peninsula flow across Larsen C. This similarity is consistent with the anticorrelation between ENSO and SAM modes previously noted (Dätwyler et al., 2020; Fogt et al., 2011). T_{max} anomalies in Figures 6c and 6e are close to zero, suggesting that SAM+ and ENSO- produce positive melt anomalies (Figures 6d and 6f) via their effect on the SEB, rather than because they raise temperatures. During SAM+ and ENSO- conditions in DJF, the SEB is dominated by SW_{\downarrow} , which causes surface melting to be

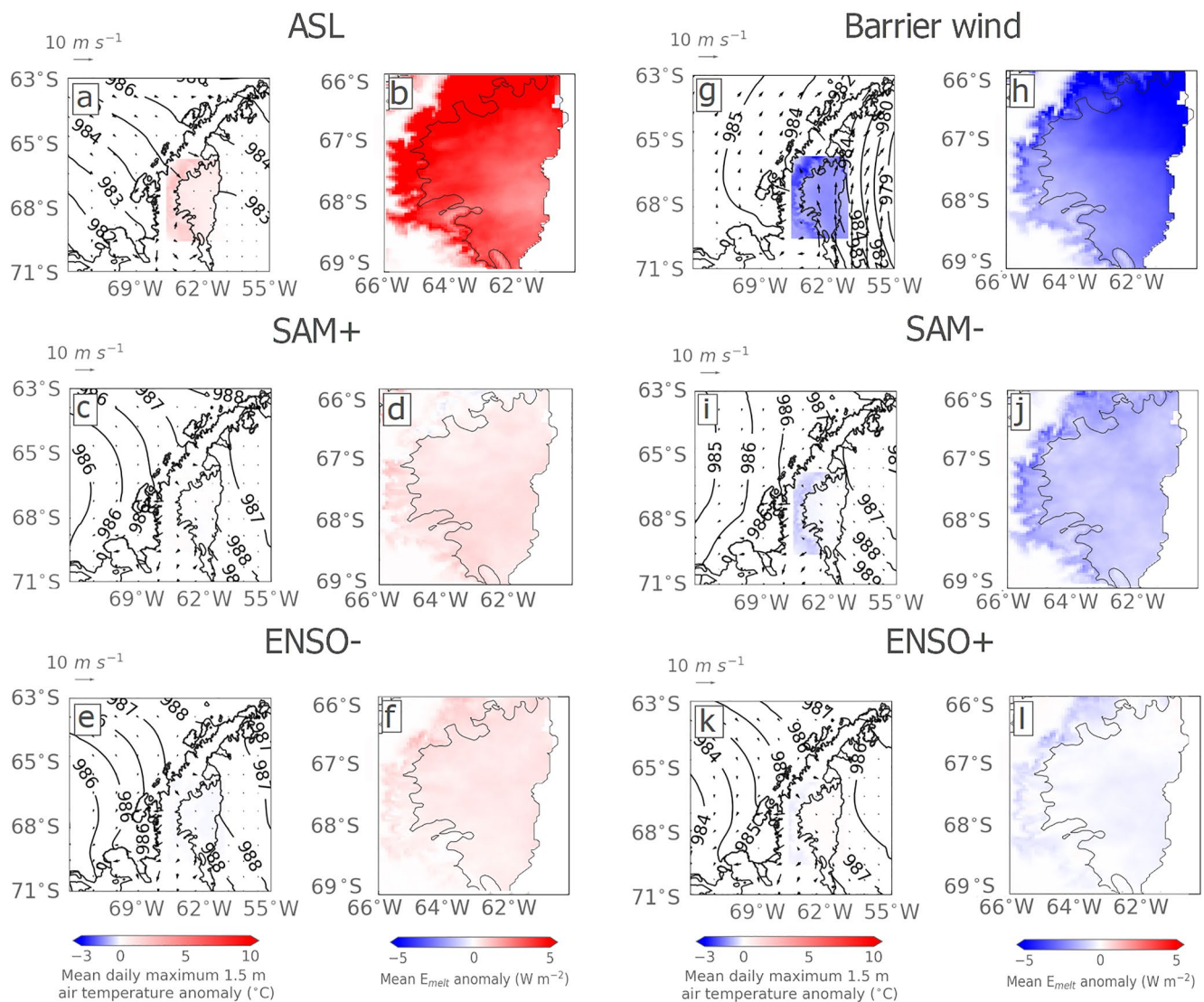


Figure 6. Composites synoptic conditions and mean E_{melt} anomalies for the large-scale circulation patterns: ASL (a, b), SAM+ (c, d), ENSO– (e, f), barrier winds (g, h), SAM– (i, j), and ENSO+ (k, l). Composites are shown for DJF only, when the absolute effect on E_{melt} is largest. Conditions that enhance melt are shown in panels a–f, while conditions that suppress melt are shown in panels g–l. Colors, vectors, and contours are as in previous figures.

widespread across the ice shelf. The synoptic conditions associated with SAM+ and ENSO– are more extreme during MAM (not shown), when intensive foehn conditions are common (as shown above), and generate positive T_{max} , H_s , and E_{melt} anomalies in inlets.

As shown in Table 2 and Figures 6a and 6b, (deep) ASL conditions are associated with positive T_{max} and E_{melt} anomalies over Larsen C during DJF and MAM. However, whereas in DJF ASL conditions are associated with positive E_{melt} anomalies across the entire shelf (Figure 6b), in MAM (not shown) the anomalies are confined to inlets with a similar pattern to the foehn composite shown in Figure 3q. Conversely, during SON and JJA ASL conditions are associated with negative T_{max} anomalies and in SON with slightly negative E_{melt} anomalies (not shown). Therefore, despite occurring 36.6% and 11.6% of the time, ASL conditions are associated with just 19.4% and 0.2% of melting during SON and JJA, respectively (Table 2).

These conditions are nonindependent and the similarities between them further suggest that SAM+, ENSO– and (in some seasons) ASL patterns produce flow-over conditions that result in foehn, the importance of which has been demonstrated. The co-occurrence of foehn and SAM+ or ENSO– conditions can also be used to demonstrate the influence of large-scale circulation patterns on mesoscale meteorology. Of the times when foehn conditions

Table 5
Pearson Correlation Coefficients Between Modeled Foehn Frequency at Inlet and Ice Shelf Stations With the Observed SAM Index for the Duration of the Hindcast

Season	Inlet	Ice shelf
DJF	0.66*	0.62*
MAM	0.55	0.54
JJA	0.19	0.16
SON	0.50	0.46
ANN	0.52	0.54

Note. Correlations that are statistically significant at the 95% level are given in bold, while statistical significance of 99% is indicated with an asterisk.

are detected, SAM+ conditions also occur 26%, 37%, 23%, and 28% of the time for SON, DJF, MAM, and JJA, respectively, while ENSO− coincides with foehn conditions 24%, 32%, 35%, and 17% of the time, respectively. This suggests that SAM+ is most important for establishing foehn conditions during DJF while ENSO− is most influential in MAM.

SAM+ has been more robustly linked to foehn occurrence, and its importance is supported by the results presented in Table 5, which shows Pearson correlation coefficients between observed SAM index and modeled foehn wind frequency at inlet and ice shelf stations for all seasons and annually, and Figure 7, which shows the relationship between these variables at inlet stations only. The correlation between annually averaged SAM index and annual mean foehn frequency is 0.52 in inlets and 0.54 at over the ice shelf (both significant at the 95% level, Table 5). This suggests that a more positive SAM index corresponds to periods of higher foehn occurrence, as also shown by, e.g., Cape et al. (2015). The largest and most significant Pearson correlation coefficient between seasonal mean SAM index and foehn occurrence (at the 99% level) is found during DJF, while it is weakest (and insignificant) during JJA. Meanwhile, those correlations in SON and MAM are significant at the 95% level (Table 5).

The composites presented in Figure 6 and the correlations between SAM+ and foehn conditions in Table 5 and Figure 7 demonstrate the importance of large-scale atmospheric circulation patterns in establishing mesoscale atmospheric conditions like foehn that promote surface melting on Larsen C.

The composites presented in Figure 6 and the correlations between SAM+ and foehn conditions in Table 5 and Figure 7 demonstrate the importance of large-scale atmospheric circulation patterns in establishing mesoscale atmospheric conditions like foehn that promote surface melting on Larsen C.

SAM and ENSO may also influence the SEB and melting via their impact on cloudiness. As noted in Section 3.2.4, foehn events can be associated with cloud clearance in some situations, and so it follows from the link between SAM+ (and by extension ENSO−) conditions and foehn occurrence that these large-scale circulation patterns could reduce cloud cover. Indeed, SAM+/ENSO− conditions are associated with negative LW_{net} anomalies and positive SW_{net} and H_s anomalies (not shown), suggesting that these conditions are associated with reduced cloud cover or thickness as well as foehn conditions. Meanwhile, during all seasons, SAM−/ENSO+ conditions are associated with the same conditions that increase cloudiness over Larsen C—notably the southeasterly flow of maritime air from over the Weddell Sea. As described in Section 3.2.3, this southeasterly airflow can enhance cloud cover and thickness, reduce SW_{\downarrow} and T_{max} , and consequently suppress E_{melt} .

3.2.6. Conditions That Suppress Melt

The focus of this study has been on conditions that enhance surface melting. However, it is evident from Table 2 and Figure 6 that some atmospheric conditions suppress melting, most notably barrier wind, SAM− and ENSO+ conditions. Low melt periods (melt amount <25th percentile) in DJF are associated with the development of a southerly barrier jet that delivers cold air from high on the Antarctic plateau, typically established by cyclones in the Weddell Sea that produce coastal easterlies or south-easterlies, resulting in cold T_{max} anomalies over Larsen C (not shown). Barrier wind conditions are associated with extremely negative T_{max} and E_{melt} anomalies across the entire Larsen C ice shelf (Figures 6g and 6h). The temperature anomalies are the primary reason that surface melting is suppressed during these periods, because E_{tot} is affected minimally (anomalies are small). SAM− (Figures 6i and 6j) and ENSO+ conditions (Figures 6k and 6l) also suppress melting relative to DJF climatology because both reduce the flow of air over the peninsula.

For all three types of melt-suppressing conditions, the magnitude of the simulated negative T_{max} anomalies is greater in nonsummer seasons, but E_{melt} anomalies are smaller because the majority of melting occurs in DJF. For instance, in nonsummer seasons ENSO+ and SAM− conditions are associated with more southerly flow which brings cold continental air over Larsen

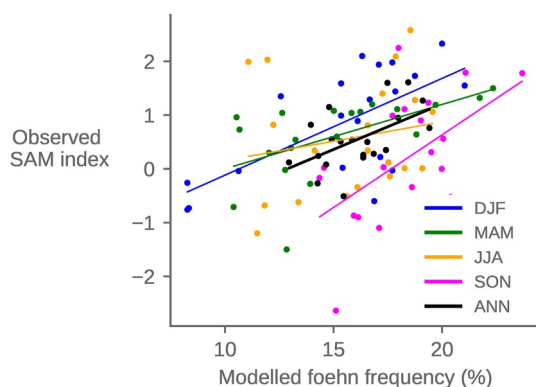


Figure 7. Scatter plot of hindcast modeled seasonal mean foehn occurrence at inlet stations, expressed as a percentage of time, against observed seasonal mean Southern Annular Mode (SAM) index for the duration of the hindcast, calculated after Marshall (2003). Individual seasons are shown with colored markers and the regression line for each season is shown in the corresponding color. The annual mean is indicated with black markers and the solid black line.

C, suppressing temperatures and melting. The exception is ENSO– conditions in SON: during these periods small positive T_{max} anomalies are simulated, which drives a very weak positive E_{melt} anomaly.

4. Summary and Conclusions

This study has comprehensively evaluated the dominant causes of surface melting on the Larsen C ice shelf in a hindcast simulation of two recent decades. Building on previous work that has explored the causes of melt on Larsen C (such as Datta et al., 2019; Elvidge et al., 2020; Gilbert et al., 2020, 2022; King et al., 2017; Kuipers Munneke et al., 2018; Wiesenekker et al., 2019), this study has systematically ranked the conditions that drive surface melt in order of importance. Many of these conditions overlap and co-occur, and so can reinforce or counteract each other (Figures 4 and 5). However, the analysis presented here has attempted to isolate the effects of individual drivers of surface melting on Larsen C. The most important drivers can be summarized as follows.

First, SW radiation is the most important driver of melting in DJF, when 90% of melting occurs. Sunny summertime conditions are associated with the highest E_{melt} anomalies of all drivers (Table 2 and Figure 3).

Second, foehn winds are the most important driver of melt in nonsummer seasons, especially MAM, but nonsummer melt only accounts for 10% of annual meltwater production (Table 2 and Figure 3). Foehn winds are also important in DJF because they enhance already-high melt fluxes, but their influence is secondary to that of SW_{\downarrow} in summer. E_{melt} anomalies are highest in all seasons when sunny and foehn conditions co-occur (Figure 4). Foehn-induced cloud clearance may drive large E_{melt} anomalies but this occurs relatively infrequently in the hindcast: rather, the occurrence of foehn during already sunny conditions enhances surface melting (Table 4).

Third, clouds—especially those with high LWP—increase LW_{\downarrow} radiation and therefore E_{tot} . However, because temperatures are typically just below the melting point during cloudy conditions, widespread melting does not regularly occur unless temperatures are already unusually high (Figure 3). This finding has important ramifications. If ongoing atmospheric warming persists, as projected throughout the 21st century, cloud-mediated melting such as is already observed in Greenland and West Antarctica could begin to occur across Larsen C and other ice shelves on the Antarctic Peninsula.

Finally, large-scale circulation patterns influence regional and mesoscale meteorology by establishing dominant flow regimes. Large-scale patterns such as SAM and ENSO as well as regional features such as the ASL and barrier winds influence atmospheric circulation in the region and can affect the surface meteorology, SEB, and melt (Figure 6). Further, large-scale circulation patterns can affect sea ice conditions, which can in turn interact with regional meteorology, for instance moderating the properties of air that flows onto the Larsen C ice shelf.

Modeled foehn frequency is shown to be strongly correlated with an observed SAM index ($r = 0.62$; Table 5 and Figure 7), which suggests that more foehn events, and therefore more melting, could result if the trend toward a more positive SAM that was recorded from the 1960–2000s (Fogt & Marshall, 2020; Marshall, 2003) resumed. While no trends in foehn frequency are evident over the hindcast period, this is likely because we only have 20 years of data and there is considerable interannual variability (cf. Gilbert et al., 2022).

The trend toward a more positive SAM is expected to resume as greenhouse gas concentrations increase. Rising greenhouse gas concentrations cause the westerly winds associated with SAM+ to strengthen and migrate polewards and will likely outweigh the compensating effects of ozone recovery if emissions continue at current levels (Zheng et al., 2013). Although future changes to ENSO are highly uncertain (Fredriksen et al., 2020), the coupling between ENSO and SAM may also imply a transition toward ENSO– conditions as the positive SAM trend continues. The combination of higher foehn frequency associated with a more positive SAM and rising temperatures related to ongoing global climate change could contribute to greater meltwater production by allowing melt to occur more frequently via the mechanisms outlined above, and for that melt to be more intense. This could lead to an eventual destabilization of Larsen C via hydrofracturing, with far-reaching implications for global sea level rise. Larsen C has already been identified as an ice shelf at risk of hydrofracturing-induced collapse if warming continues unchecked (Gilbert & Kittel, 2021; Trusel et al., 2015). Quantifying the future fate of the Larsen C ice shelf is beyond the scope of this paper but should be a focus of research to determine change on the Antarctic Peninsula.

Conflict of Interest

The authors declare no conflicts of interest relevant to this study.

Data Availability Statement

Hindcast model data can be accessed on the CEDA archive at <https://catalogue.ceda.ac.uk/uuid/41c879b06af642e-9bc8e12d1d0ea3d62> and can be cited as Gilbert, E. (2020): High-resolution regional Met Office Unified Model (UM) climate model hindcast of the Antarctic Peninsula (1998–2017). Centre for Environmental Data Analysis, date of citation. AWS data can be retrieved from <https://www.projects.science.uu.nl/iceclimate/aws/>.

Acknowledgments

This work was supported by the Natural Environment Research Council through the EnvEast Doctoral Training Partnership (Grant NE/L002582/1). The authors also acknowledge use of the MONSOon system, a collaborative facility supplied under the Joint Weather and Climate Research Programme, a strategic partnership between the Met Office and the Natural Environment Research Council. The authors gratefully acknowledge Prof. Michiel R. van den Broeke, who kindly provided AWS data. The authors are grateful to R. T. Datta and one anonymous reviewer for helpful comments on an earlier version of this manuscript.

References

- Bell, R. E., Banwell, A. F., Trusel, L. D., & Kingslake, J. (2018). Antarctic surface hydrology and impacts on ice-sheet mass balance. *Nature Climate Change*, 8, 1044–1052. <https://doi.org/10.1038/s41558-018-0326-3>
- Bennartz, R., Shupe, M. D., Turner, D. D., Walden, V. P., Steffen, K., Cox, C. J., et al. (2013). July 2012 Greenland melt extent enhanced by low-level liquid clouds. *Nature*, 496(7443), 83–86. <https://doi.org/10.1038/nature12002>
- Bevan, S. L., Luckman, A. J., Kuipers Munneke, P., Hubbard, B., Kulesa, B., & Ashmore, D. W. (2018). Decline in surface melt duration on Larsen C ice shelf revealed by the Advanced Scatterometer (ASCAT). *Earth and Space Science*, 5, 578–591. <https://doi.org/10.1029/2018EA000421>
- Bozkurt, D., Bromwich, D. H., Carrasco, J., Hines, K. M., Maureira, J. C., & Rondanelli, R. (2020). Recent near-surface temperature trends in the Antarctic Peninsula from observed, reanalysis and regional climate model data. *Advances in Atmospheric Sciences*, 37, 477–493. <https://doi.org/10.1007/s00376-020-9183-x>
- Cape, M. R., Vernet, M., Skvarca, P., Marinsek, S., Scambos, T., & Domack, E. (2015). Foehn winds link climate-driven warming to ice shelf evolution in Antarctica. *Journal of Geophysical Research: Atmospheres*, 120, 11037–11111. <https://doi.org/10.1002/2015JD023465>
- Center for Climate Prediction. (2005). *Teleconnection pattern calculation procedures*. Retrieved from https://www.cpc.ncep.noaa.gov/products/precip/CWlink/daily_ao_index/history/method.shtml
- Clem, K. R., Renwick, J. A., McGregor, J., & Fogt, R. L. (2016). The relative influence of ENSO and SAM on Antarctic Peninsula climate. *Journal of Geophysical Research: Atmospheres*, 121, 11038–11054. <https://doi.org/10.1002/2016JD025305>
- Datta, R. T., Tedesco, M., Fettweis, X., Agosta, C., Lhermitte, S., Lenaerts, J. T. M., & Wever, N. (2019). The effect of foehn-induced surface melt on firn evolution over the Northeast Antarctic Peninsula. *Geophysical Research Letters*, 46, 3822–3831. <https://doi.org/10.1029/2018GL080845>
- Dätwyler, C., Grosjean, M., Steiger, N. J., & Neukom, R. (2020). Teleconnections and relationship between ENSO and SAM in reconstructions and models over the past millennium. *Climate of the Past*, 743, 743–756. <https://doi.org/10.5194/cp-16-743-2020>
- Deb, P., Orr, A., Bromwich, D. H., Nicolas, J. P., Turner, J., & Hosking, J. S. (2018). Summer drivers of atmospheric variability affecting ice shelf thinning in the Amundsen Sea Embayment, west Antarctica. *Geophysical Research Letters*, 45, 4124–4133. <https://doi.org/10.1029/2018GL077092>
- Dee, D. P., Uppala, S. M., Simmons, A. J., Berrisford, P., Poli, P., Kobayashi, S., et al. (2011). The ERA-Interim reanalysis: Configuration and performance of the data assimilation system. *Quarterly Journal of the Royal Meteorological Society*, 137(656), 553–597. <https://doi.org/10.1002/qj.828>
- Elvidge, A. D., Kuipers Munneke, P., King, J. C., Renfrew, I. A., & Gilbert, E. (2020). Atmospheric drivers of melt on Larsen C ice shelf: Surface energy budget regimes and the impact of foehn. *Journal of Geophysical Research: Atmospheres*, 125, e2020JD032463. <https://doi.org/10.1029/2020JD032463>
- Elvidge, A. D., Renfrew, I. A., King, J. C., Orr, A., & Lachlan-Cope, T. A. (2016). Foehn warming distributions in nonlinear and linear flow regimes: A focus on the Antarctic Peninsula. *Quarterly Journal of the Royal Meteorological Society*, 142(695), 618–631. <https://doi.org/10.1002/qj.2489>
- Elvidge, A. D., Renfrew, I. A., King, J. C., Orr, A., Lachlan-Cope, T. A., Weeks, M., & Gray, S. L. (2015). Foehn jets over the Larsen C ice shelf, Antarctica. *Quarterly Journal of the Royal Meteorological Society*, 141(688), 698–713. <https://doi.org/10.1002/qj.2382>
- Fogt, R. L., Bromwich, D. H., & Hines, K. M. (2011). Understanding the SAM influence on the South Pacific ENSO teleconnection. *Climate Dynamics*, 36(7), 1555–1576. <https://doi.org/10.1007/s00382-010-0905-0>
- Fogt, R. L., & Marshall, G. J. (2020). The Southern Annular Mode: Variability, trends, and climate impacts across the southern Hemisphere. *WIREs Climate Change*, 11(4), e652. <https://doi.org/10.1002/wcc.652>
- Fredriksen, H. B., Berner, J., Subramanian, A. C., & Capotondi, A. (2020). How does El Niño–Southern Oscillation change under global warming—A first look at CMIP6. *Geophysical Research Letters*, 47, e2020GL090640. <https://doi.org/10.1029/2020GL090640>
- Ghiz, M., Scott, R., Vogelmann, A., Lenaerts, J., Lazzara, M., & Lubin, D. (2021). Energetics of surface melt in West Antarctica. *The Cryosphere*, 15, 3459–3494. <https://doi.org/10.5194/tc-15-3459-2021>
- Gilbert, E. (2020a). *High-resolution regional Met Office Unified Model (UM) climate model hindcast of the Antarctic Peninsula (1998–2017)*. Centre for Environmental Data Analysis. Retrieved from <https://catalogue.ceda.ac.uk/uuid/41c879b06af642e9bc8e12d1d0ea3d62>
- Gilbert, E. (2020b). *Atmospheric drivers of surface melting on the Larsen C ice shelf, Antarctic Peninsula* (PhD thesis). University of East Anglia.
- Gilbert, E., & Kittel, C. (2021). Surface melt and runoff on Antarctic ice shelves at 1.5°C, 2°C and 4°C of future warming. *Geophysical Research Letters*, 48, e2020GL091733. <https://doi.org/10.1029/2020GL091733>
- Gilbert, E., Orr, A., King, J. C., Renfrew, I. A., & Lachlan-Cope, T. (2022). A 20-year study of melt processes over Larsen C ice shelf using a high-resolution regional atmospheric model: Part 1, model configuration and validation. *Journal of Geophysical Research: Atmospheres*. <https://doi.org/10.1002/essoar.10506250.1>
- Gilbert, E., Orr, A., King, J. C., Renfrew, I. A., Lachlan-Cope, T., Field, P. F., & Boutle, I. A. (2020). Summertime cloud phase strongly influences surface melting on the Larsen C ice shelf, Antarctica. *Quarterly Journal of the Royal Meteorological Society*, 146(729), 1575–1589. <https://doi.org/10.1002/qj.3753>
- Grosvenor, D. P., King, J. C., Choularton, T. W., & Lachlan-Cope, T. (2014). Downslope foehn winds over the Antarctic Peninsula and their effect on the Larsen ice shelves. *Atmospheric Chemistry and Physics*, 14(18), 9481–9509. <https://doi.org/10.5194/acp-14-9481-2014>

- Hofer, S., Tedstone, A. J., Fettweis, X., & Bamber, J. (2019). Cloud microphysics and circulation anomalies control differences in future Greenland melt. *Nature Climate Change*, 9, 523–528. <https://doi.org/10.1038/s41558-019-0507-8>
- Hoinka, K. P. (1985). What is a foehn clearance? *Bulletin of the American Meteorological Society*, 66(9), 1123–1132. [https://doi.org/10.1175/1520-0477\(1985\)066<1123:wiafc>2.0.co;2](https://doi.org/10.1175/1520-0477(1985)066<1123:wiafc>2.0.co;2)
- Hosking, J. S., Orr, A., Marshall, G. J., Turner, J., & Phillips, T. (2013). The influence of the Amundsen-Bellinghousen seas low on the climate of West Antarctica and its representation in coupled climate model simulations. *Journal of Climate*, 26(17), 6633–6648. <https://doi.org/10.1175/JCLI-D-12-00813.1>
- Kay, J. E., L'Ecuyer, T., Gettelman, A., Stephens, G., & O'Dell, C. (2008). The contribution of cloud and radiation anomalies to the 2007 Arctic sea ice extent minimum. *Geophysical Research Letters*, 35(8), 1–5. <https://doi.org/10.1029/2008gl033451>
- King, J. C. (1994). Recent climate variability in the vicinity of the Antarctic Peninsula. *International Journal of Climatology*, 14, 357–369. <https://doi.org/10.1002/joc.3370140402>
- King, J. C., Gadian, A., Kirchgassner, A., Kuipers Munneke, P., Lachlan-Cope, T. A., Orr, A., et al. (2015). Validation of the summertime surface energy budget of Larsen C Ice Shelf (Antarctica) as represented in three high-resolution atmospheric models. *Journal of Geophysical Research: Atmospheres*, 120, 1335–1347. <https://doi.org/10.1002/2014JD022604>
- King, J. C., Kirchgassner, A., Orr, A., Luckman, A., Bevan, S., Elvidge, A., et al. (2017). The impact of foehn winds on surface energy balance and melt over Larsen C Ice Shelf, Antarctica. *Journal of Geophysical Research: Atmospheres*, 122, 12062–12112. <https://doi.org/10.1002/2017JD026809>
- Kuipers Munneke, P., Luckman, A. J., Bevan, S. L., Gilbert, E., Smeets, C. J. P. P., Van Den Broeke, M. R., et al. (2018). Intense winter surface melt on an Antarctic ice shelf. *Geophysical Research Letters*, 45, 7615–7623. <https://doi.org/10.1029/2018GL077899>
- Kuipers Munneke, P., Van Den Broeke, M. R., King, J. C., Gray, T., & Reijmer, C. H. (2012). Near-surface climate and surface energy budget of Larsen C ice shelf, Antarctic Peninsula. *The Cryosphere*, 6(2), 353–363. <https://doi.org/10.5194/tc-6-353-2012>
- Laffin, M. K., Zender, C. S., Singh, S., Van Wessem, J. M., Smeets, C. J. P. P., & Reijmer, C. H. (2021). Climatology and evolution of the Antarctic Peninsula föhn wind-induced melt regime from 1979–2018. *Journal of Geophysical Research: Atmospheres*, 126, e2020JD033682. <https://doi.org/10.1029/2020JD033682>
- Lai, C. Y., Kingslake, J., Wearing, M. G., Chen, P. H. C., Gentine, P., Li, H., et al. (2020). Vulnerability of Antarctica's ice shelves to meltwater-driven fracture. *Nature*, 584(7822), 574–578. <https://doi.org/10.1038/s41586-020-2627-8>
- Liu, H., Jezek, K. C., Li, B., & Zhao, Z. (2015). *RadarSat Antarctic Mapping Project Digital Elevation Model, Version 2. NSIDC; NASA National Snow and Ice Data Center distributed active archive center*. <https://doi.org/10.5067/8JKNEW6BFRVD>
- Marshall, G. J. (2003). Trends in the Southern Annular Mode from observations and reanalyses. *Journal of Climate*, 16(24), 4134–4143. [https://doi.org/10.1175/1520-0442\(2003\)016<4134:TITSAM>2.0.CO;2](https://doi.org/10.1175/1520-0442(2003)016<4134:TITSAM>2.0.CO;2)
- Marshall, G. J., Orr, A., van Lipzig, N. P. M., & King, J. C. (2006). The impact of a changing Southern Hemisphere annular mode on Antarctic Peninsula summer temperatures. *Journal of Climate*, 19(20), 5388–5404. <https://doi.org/10.1175/JCLI3844.1>
- Orr, A., Cresswell, D., Marshall, G. J., Hunt, J. C. R., Sommeria, J., Wang, C. G., & Light, M. (2004). A 'low-level' explanation for the recent large warming trend over the Western Antarctic Peninsula involving blocked winds and changes in zonal circulation. *Geophysical Research Letters*, 31, L06204. <https://doi.org/10.1029/2003GL019160>
- Orr, A., Kirchgassner, A., King, J., Phillips, T., Gilbert, E., Elvidge, A., et al. (2021). Comparison of kilometre and sub-kilometre scale simulations of a foehn wind event over the Larsen C ice shelf using the Met Office Unified model (MetUM). *Quarterly Journal of the Royal Meteorological Society*, 147, 3472–3492. <https://doi.org/10.1002/qj.4138>
- Orr, A., Marshall, G. J., Hunt, J. C. R., Sommeria, J., Wang, C.-G., & van Lipzig, N. P. M. (2008). Characteristics of summer airflow over the Antarctic Peninsula in response to recent strengthening of westerly circumpolar winds. *Journal of the Atmospheric Sciences*, 65(4), 1396–1413. <https://doi.org/10.1175/2007JAS2498.1>
- Parish, T. R. (1983). The influence of the Antarctic Peninsula on the wind field over the Western Weddell Sea. *Journal of Geophysical Research*, 88, 2684–2692. <https://doi.org/10.1029/JC088iC04p02684>
- Reynolds, R. W., Smith, T. M., Liu, C., Chelton, D. B., Casey, K. S., & Schlax, M. G. (2007). Daily high-resolution-blended analyses for sea surface temperature. *Journal of Climate*, 20(22), 5473–5496. <https://doi.org/10.1175/2007JCLI1824.1>
- Scambos, T., Hulbe, C., & Fahnestock, M. (2003). Climate-induced ice shelf disintegration in the Antarctic Peninsula. In E. Domack, A. Levente, A. Burnet, R. Bindshadler, P. Convey, & M. Kirby (Eds.), *Antarctic Peninsula climate variability: Historical and paleoenvironmental perspectives* (Vol. 79, pp. 79–92). <https://doi.org/10.1029/AR079p0079>
- Scambos, T. A., Hulbe, C., Fahnestock, M., & Bohlander, J. (2000). The link between climate warming and break-up of ice shelves in the Antarctica Peninsula. *Journal of Glaciology*, 46(154), 516–530. <https://doi.org/10.3189/172756500781833043>
- Schwerdtfeger, W. (1974). Mountain barrier effect on the flow of stable air north of the Brooks Range. In *Proceedings of the 24th Alaskan Science Conference* (pp. 204–208). [https://doi.org/10.1175/1520-0493\(1975\)103<0045:TEOTAP>2.0.CO;2](https://doi.org/10.1175/1520-0493(1975)103<0045:TEOTAP>2.0.CO;2)
- Siegert, M., Atkinson, A., Banwell, A., Brandon, M., Convey, P., Davies, B., et al. (2019). The Antarctic Peninsula under a 1.5°C global warming scenario. *Frontiers in Environmental Science*, 7, 102. <https://doi.org/10.3389/fenvs.2019.00102>
- Takane, Y., & Kusaka, H. (2011). Formation mechanisms of the extreme high surface air temperature of 40.9°C observed in the Tokyo metropolitan area: Considerations of dynamic foehn and foehnlike wind. *Journal of Applied Meteorology and Climatology*, 50(9), 1827–1841. <https://doi.org/10.1175/JAMC-D-10-05032.1>
- Trusel, L. D., Frey, K. E., Das, S. B., Karnauskas, K. B., Kuipers Munneke, P., van Meijgaard, E., & van den Broeke, M. R. (2015). Divergent trajectories of Antarctic surface melt under two twenty-first-century climate scenarios. *Nature Geoscience*, 8(12), 927–932. <https://doi.org/10.1038/ngeo2563>
- Turner, J., Phillips, T., Hosking, J. S., Marshall, G. J., & Orr, A. (2013). The Amundsen Sea Low. *International Journal of Climatology*, 33(7), 1818–1829. <https://doi.org/10.1002/joc.3558>
- Turton, J. V., Kirchgassner, A., Ross, A., King, J., & Kuipers Munneke, P. (2020). The influence of föhn winds on annual and seasonal surface melt on the Larsen C Ice Shelf, Antarctica. *The Cryosphere Discussions*, 14, 4165–4180. <https://doi.org/10.5194/tc-14-4165-2020>
- Turton, J. V., Kirchgassner, A., Ross, A. N., & King, J. C. (2018). The spatial distribution and temporal variability of föhn winds over the Larsen C ice shelf, Antarctica. *Quarterly Journal of the Royal Meteorological Society*, 144(713), 1169–1178. <https://doi.org/10.1002/qj.3284>
- van Lipzig, N. P. M., Marshall, G. J., Orr, A., & King, J. C. (2008). The relationship between the Southern Hemisphere annular mode and Antarctic Peninsula summer temperatures: Analysis of a high-resolution model climatology. *Journal of Climate*, 21(8), 1649–1668. <https://doi.org/10.1175/2007JCLI1695.1>
- van Oldenborgh, G. J., Collins, M., Arblaster, J., Christensen, J. H., Marotzke, J., & Power, S. B. (2013). Atlas of global and regional climate projections. In T. F. Stocker, D. Qin, G.-K. Plattner, M. Tignor, S. K. Allen, & J. Boschung (Eds.), *Climate change 2013: The physical science*

- basis. *Contribution of working group I to the fifth assessment report of the Intergovernmental Panel on Climate Change* (pp. 1311–1394). Cambridge University Press. <https://doi.org/10.1017/CBO9781107415324.029>
- Van Wessem, J. M., Ligtenberg, S. R. M., Reijmer, C. H., Van De Berg, W. J., Van Den Broeke, M. R., Barrand, N. E., et al. (2016). The modelled surface mass balance of the Antarctic Peninsula at 5.5 km horizontal resolution. *The Cryosphere*, *10*(1), 271–285. <https://doi.org/10.5194/tc-10-271-2016>
- Van Wessem, J. M., Reijmer, C. H., Van De Berg, W. J., Van Den Broeke, M. R., Cook, A. J., Van Uft, L. H., & Van Meijgaard, E. (2015). Temperature and wind climate of the Antarctic Peninsula as simulated by a high-resolution regional atmospheric climate model. *Journal of Climate*, *28*(18), 7306–7326. <https://doi.org/10.1175/JCLI-D-15-0060.1>
- Wiesenekker, J. M., Munneke, P. K., van den Broeke, M. R., & Paul Smeets, C. J. P. (2019). A multidecadal analysis of Föhn winds over Larsen C ice shelf from a combination of observations and modeling. *Atmosphere*, *9*(5), 172. <https://doi.org/10.3390/atmos9050172>
- Zhang, T., Starnes, K., & Bowling, S. A. (1996). Impact of clouds on surface radiative fluxes and snowmelt in the arctic and subarctic. *Journal of Climate*, *9*(9), 2110–2123. [https://doi.org/10.1175/1520-0442\(1996\)009<2110:IOCOSR>2.0.CO;2](https://doi.org/10.1175/1520-0442(1996)009<2110:IOCOSR>2.0.CO;2)
- Zheng, F., Li, J., Clark, R. T., & Nnamchi, H. C. (2013). Simulation and projection of the Southern Hemisphere annular mode in CMIP5 models. *Journal of Climate*, *26*(24), 9860–9879. <https://doi.org/10.1175/JCLI-D-13-00204.1>